LAWRENCE
LIVERMORE
NATIONAL
LABORATORY

LLNL-CONF-680615

Generalized Lawson Criteria for Inertial Confinement Fusion

R. E. Tipton

January 6, 2016

Inertial Fusion Science Application
Seattle, WA, United States
September 21, 2015 through September 25, 2015

Disclaimer

Generalized Lawson Criteria for Inertial Confinement Fusion

Robert Tipton

Lawrence Livermore National Laboratory, Livermore California USA

tipton1@llnl.gov

Abstract. The Lawson Criterion was proposed by John D. Lawson in 1955 as a general measure of the conditions necessary for a magnetic fusion device to reach thermonuclear ignition. Over the years, similar ignition criteria have been proposed which would be suitable for Inertial Confinement Fusion (ICF) designs. This paper will compare and contrast several ICF ignition criteria based on Lawson's original ideas. Both analytical and numerical results will be presented which will demonstrate that although the various criteria differ in some details, they are closely related and perform similarly as ignition criteria. A simple approximation will also be presented which allows the inference of each ignition parameter directly from the measured data taken on most shots fired at the National Ignition Facility (NIF) with a minimum reliance on computer simulations. Evidence will be presented which indicates that the experimentally inferred ignition parameters on the best NIF shots are approaching the ignition threshold.

1. Introduction

In 1955 John Lawson proposed several ignition criteria for deuterium-tritium (DT) plasma in a magnetic fusion device[1]. The more famous was $n\tau > 1.5x10^{14}$ *sec/cc* – where n is the DT plasma density in atoms/cc and τ is the plasma confinement time in seconds. The less famous but more useful criterion was the triple product: $nT\tau > 3x10^{15}$ *KeV-sec/cc* – where T is the temperature of the DT plasma in KeV. The triple product can easily be expressed as pressure times τ or $P\tau > 9.6$ atm-sec. The exact threshold values for both criteria are dependent on the temperature of the plasma.

While the Lawson criteria were originally designed for magnetically confined fusion plasmas, many people saw the value of generalizing Lawson's original criteria to the context of Inertial Confinement Fusion (ICF). One such example is the work of Ricardo Betti who published a $P\tau$ or χ criterion in 2010[2] which is essentially the same as Lawson's Triple Product $nT\tau$.

Baolian Cheng[3] and others have taken Lawson's Triple Product and derived ignition criteria with the following form:

$$\rho RT^n > Threshold$$

In this paper it will be shown that the ignition criterion of Heiner Meldner can also be expressed in this same form.

The Lawrence Livermore National Laboratory (LLNL) has developed another useful ignition criteria known as the Ignition Threshold Factor Experimental or ITFX[4]:

$$ITFX = \left(\frac{Y_n}{4.0 \times 10^{15}}\right)\left(\frac{DSR}{0.067}\right)^{2.1} > 1.0$$

Yn is the measured neutron yield of the shot and DSR is the measured Down Scattered Ratio which is the number of measured neutrons between 10 and 12 MeV divided by the number of measured neutrons between 13 and 15 MeV. It has been shown[2][4] that a generalization of Betti's χ criterion is closely related to ITFX.

Hence we see that all of ignition parameters in use today are generalizations of Lawson's original criterion. Section 2 will describe Betti's generalization of Lawson's Triple Product into the χ ignition parameter. Section 3 will describe the derivation of Cheng's ignition parameter and generalize it for the tamping effect of the cold DT ice. Section 4 will describe the work of Heiner Meldner and also generalize it for the tamping effect of the cold DT ice.

Section 5 will present a simple set of approximations originally due to Springer and Cerjan[5] which allow the various ignition parameters to be directly inferred from measured NIF data without relying computer simulations. Section 6 will use numerical simulations of a NIF ignition capsule to show how the various ignition parameters perform as ignition parameters. Section 7 will present the inferred ignition parameters from a number of NIF shots and section 8 will finish up with a summary.

2. Lawson's Fundamental Assumption and Betti's χ

We start with Lawson's fundamental hypothesis which is that ignition occurs when the thermonuclear energy deposition rate exceeds the plasma energy dissipation rate:

$$\dot{E}_{TN} = n^2 \chi_D \chi_T \langle \sigma v(T) \rangle K_B T_\alpha > \frac{E_{Plasma}}{\tau}$$

$\dot{E}_{TN}$ is the thermonuclear energy deposition rate (energy/volume/time) assuming all of the alpha energy is instantly thermalized and all of the neutron energy escapes. n is the plasma ion density. χ_D and χ_T are the atom fractions of deuterium and tritium. $T_\alpha = 3541\, KeV$ is the energy of the thermonuclear alpha particle. $K_B = 1.60217657 \times 10^{-9}$ is the constant necessary to convert KeV into ergs. $\langle \sigma v(T) \rangle$ is the thermonuclear cross-section averaged over a Maxwellian distribution of temperature, T. $E_{Plama} = 2\left(\frac{3}{2} n K_B T\right)$ is the thermal energy of the plasma (energy/volume) and τ is the energy dissipation time (or the plasma confinement time).

Lawson's fundamental assumption can be rearranged to give the $n\tau$ criterion and the triple product criterion:

$n\tau$ Criterion $$n\tau > \frac{12}{T_\alpha}\frac{T}{\langle \sigma v \rangle}\left[\frac{1}{4\chi_D \chi_T}\right]$$

Triple Product Criterion $$nT\tau > \frac{12}{T_\alpha}\frac{T^2}{\langle \sigma v \rangle}\left[\frac{1}{4\chi_D \chi_T}\right]$$

The plasma pressure is simply $P = 2K_B nT$. This allows us to rewrite the triple product criterion as the Pτ criterion.

Pτ Criterion $$P\tau > \frac{24K_B}{T_\alpha}\left(\frac{T^2}{\langle\sigma v\rangle}\right)\left[\frac{1}{4\chi_D\chi_T}\right]$$

The problem with the Pτ criterion is that the exact value of the ignition threshold is a function of the hot spot temperature. A better measure of ignition threshold was introduced by Ricardo Betti[2]. This ignition parameter – known as χ – is formed by dividing Pτ by the function of temperature on the other side of the inequality in the equation above which will be labelled $(P\tau)_{ig}$. The ignition condition in terms of χ is simply that χ > 1.

$$(P\tau)_{ig} = \frac{24K_B}{T_\alpha}\left(\frac{T^2}{\langle\sigma v(T)\rangle}\right)\left[\frac{1}{4\chi_D\chi_T}\right]$$

$$\chi = \frac{P\tau}{(P\tau)_{ig}} > 1$$

3. Cheng's Ignition Parameter

Baolian Cheng and her co-authors[3], start with the Lawson's triple product and then rearrange the terms to get:

$$\rho T^2\tau > \frac{12A_{DT}}{N_0 T_\alpha}\frac{T^3}{\langle\sigma v\rangle}\left[\frac{0.8\chi_D + 1.2\chi_T}{4\chi_D\chi_T}\right]$$

Cheng et al took τ to be the speed-of-sound transit time across the bare hot spot. It is more accurate to replace τ by the speed-of-sound transit time across both the hot spot and the cold fuel:

$$\tau = \frac{R}{C_h} + \frac{\Delta R}{C_c} = \frac{R}{C_h}\left(1 + \frac{\Delta R C_h}{R C_c}\right)$$

R is the radius of the hot spot. ΔR is the radial thickness of the cold fuel. C_h is the speed of sound in the hot spot and C_c is the speed of sound in the cold fuel. Assuming the hot spot and cold fuel are in pressure equilibrium and assuming the hot spot speed of sound is well described by the fully ionized ideal gas law and the cold fuel speed of sound is well described by Fermi-degenerate equation of state, it is straightforward to transform the expression for τ.

$$\tau = \frac{R}{C_h}\left(1 + \frac{\rho_c \Delta R}{\rho R}\sqrt{\frac{\rho}{\rho_c}}\right)$$

ρ is the density of the hot spot and ρ_c is the density of the cold fuel. Substituting this expression for τ into the $\rho T^2\tau$ condition at the top of this section gives:

$$\rho R T^2 > \frac{12}{T_\alpha}\sqrt{\frac{2\gamma A_{DT} K_B}{N_0}}\frac{T^{3.5}}{\langle\sigma v\rangle}\left\{\frac{1}{1 + \frac{\rho_c \Delta R}{\rho R}\sqrt{\frac{\rho}{\rho_c}}}\right\}\left[\frac{\sqrt{0.8\chi_D + 1.2\chi_T}}{4\chi_D\chi_T}\right]$$

For temperatures between 2 and 4 KeV, $\langle \sigma v \rangle$ can be approximated by a power law which allows this ignition condition to be further simplified.

$$\rho R T^2 > \frac{12.6172}{T^{0.09}} \left\{ \frac{1}{1 + \frac{\rho_c \Delta R}{\rho R} \sqrt{\frac{\rho}{\rho_c}}} \right\} \left[\frac{\sqrt{0.8\chi_D + 1.2\chi_T}}{4\chi_D \chi_T} \right]$$

Finally just as with Betti's χ, we define a new ignition parameter which we will call β as ρRT^2 divided by the right side of the expression above. The expression for β and the ignition condition for β are given here:

$$\beta = \frac{\rho R T^2}{12.6172} T^{0.09} \left\{ 1 + \frac{\rho_c \Delta R}{\rho R} \sqrt{\frac{\rho}{\rho_c}} \right\} \left[\frac{4\chi_D \chi_T}{\sqrt{0.8\chi_D + 1.2\chi_T}} \right] > 1$$

4. Meldner's Problem and Related Ignition Parameter

Heiner Meldner was an ICF scientist at Livermore during the 1970's and 1980's. He used ICF codes to map out the ignition conditions of hot spots under various conditions. He mapped out the ignition conditions for bare hot spots and for hot spots surrounded by a heavy gold pusher found in most double-shell designs.

It is straightforward to generalize Meldner's approach for a hot spot surrounded by cold fuel which we will assume is in pressure equilibrium with the hot spot. It takes 5 numbers to describe the hot spot + cold fuel combination which we will take to be:

M_{DT}	The total D+T mass of the hot spot and cold fuel
α	The pressure degeneracy ratio P/P_{Fermi}
M_f	The ratio of the hot spot mass to the total DT mass
ρR	The rR of the hot spot
T	The temperature of the hot spot

Numerical simulations show that the ignition threshold is only weakly sensitive to the total DT mass M_{DT} or the pressure degeneracy ratio α. As a consequence we will focus on the ignition threshold as a function of the three remaining parameters. Figure 4.1 shows the calculated ignition threshold for the Meldner problem as a function of hot spot mass fraction M_f, the hot spot ρR and the hot spot T.

The ignition curves for different hot spot mass fractions are plotted in the plane of hot spot ρR and hot spot temperature. The curve with the mass fraction of unity is Meldner's prediction of the ignition conditions for a bare sphere of DT plasma with a given ρR and temperature. The ignition threshold curves are lower for mass fractions less than unity due to the effect of inertial tamping arising from the presence of the cold DT fuel. A typical DT layered shot on NIF has a hot spot mass fraction of around 2%.

It is interesting to compare the numerically generated ignition curves from the Meldner problem with the ignition conditions of section 3 following the philosophy of Baolian Cheng. Figure 4.2 plots the Meldner ignition thresholds in red and the analytic ignition thresholds of section 3 in blue. The two sets of curves are similar but there are clear differences.

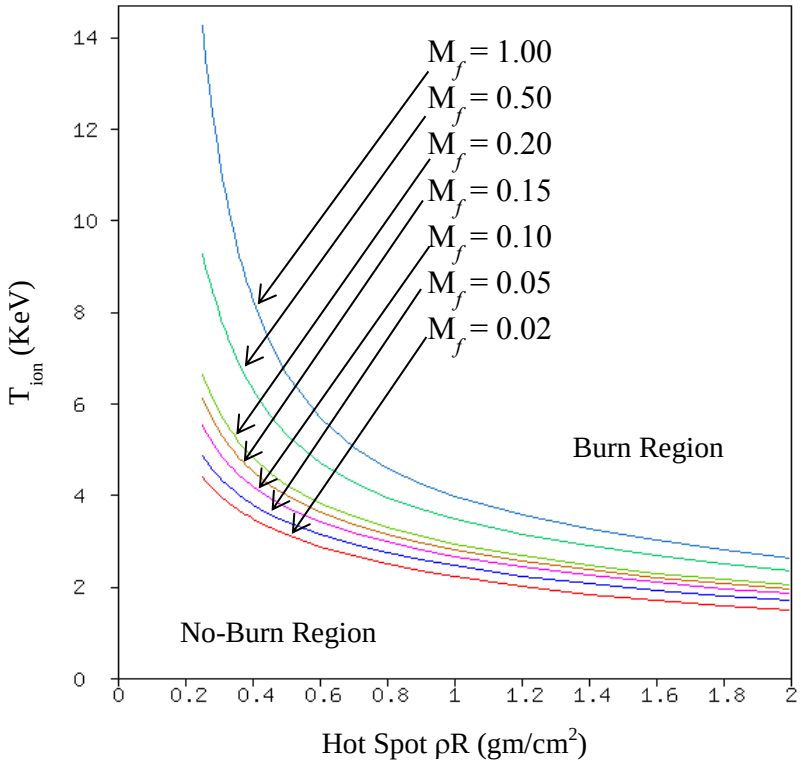

Figure 4.1: Ignition Threshold for Meldner Problem

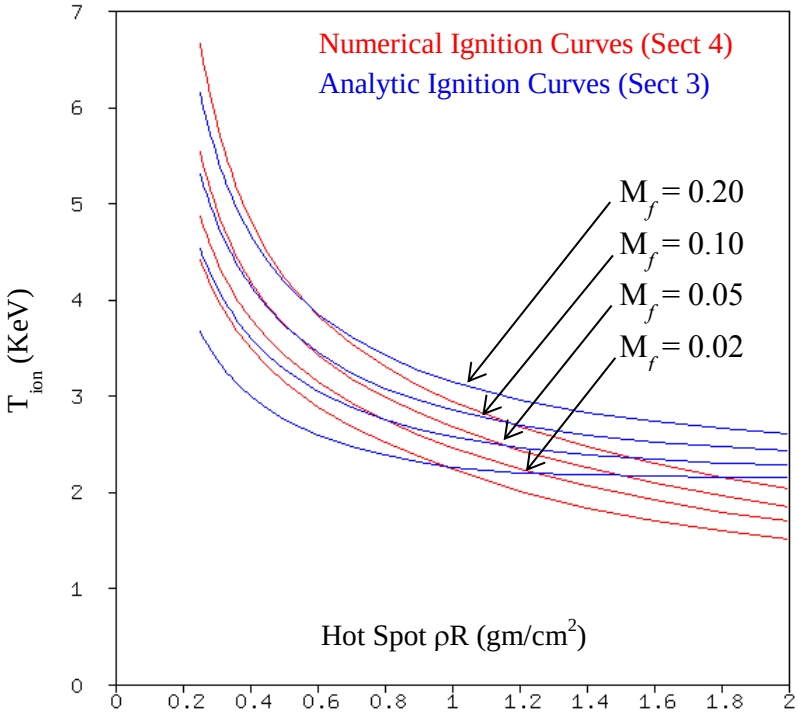

Figure 4.2: Numerical Ignition Thresholds (red) compared with Analytic Thresholds (blue).

The analytic curves are the results of many approximations and assumptions whereas the only significant assumption of the numerical curves is spherical symmetry. For this reason, the numerical Meldner curves are like to be more accurate than the analytic curves. It is productive to produce a simple fit to the Meldner curves which is given here:

$$\rho RT^2 = 14.2478 M_f^{0.2831}$$

Figure 4.3 compares the numerical Meldner curves with the simple fit. The simple fit isn't perfect but it's not bad. Given that the numerical ignition curves are likely to be more accurate than the analytic ignition curves, we will redefine the ignition parameter β as follows:

$$\beta = \frac{\rho RT^2}{14.2478 M_f^{0.2831}} > 1$$

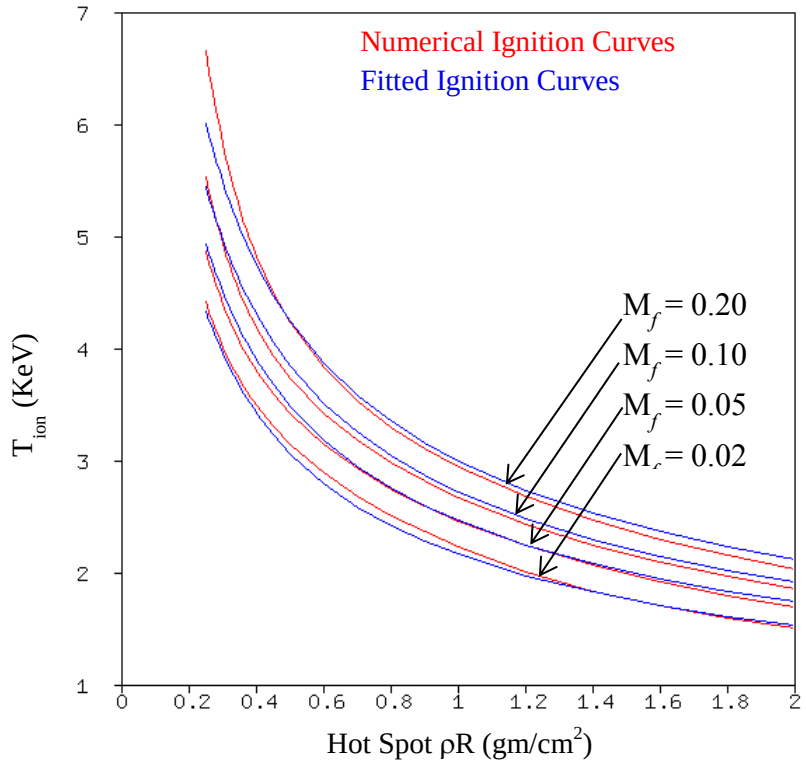

Figure 4.3: Numerical Ignition Thresholds (red) compared with simple fit (blue).

5. Experiment Measurement of Ignition Parameters

It is possible to infer each of the ignition parameters discussed in this paper directly from measured data taken on most NIF shots. This inference can be made without relying on detailed simulations of ICF codes. The methodology of how to take measured NIF data and infer the hot spot conditions was first proposed by Paul Springer and Charlie Cerjan[5].

We start with 5 basic measurements taken on most layered DT shots fired on the NIF:

Yn	Neutron yield (measured neutrons 13-15 MeV)
T	Hot spot average ion temperature (NTOF Brysk Temperature)
RHS	Hot spot radius (P_0 of the 17% contour of the neutron pinhole image)
τ	Burn duration (FWHM of the TN gamma signal)
DSR	Down Scattered Ratio (neutrons 10-12 MeV/ 13-15 MeV)

The fundamental assumption of Springer and Cerjan is that the neutron yield can be related to the fundamental properties of the hot spot by a simple relation.

$$Y_n = n_{ion}^2 \chi_D \chi_T \langle \sigma v(T) \rangle \tau \frac{4\pi}{3} R_{HS}^3$$

Every term in the above expression can be measured except for the ion density of the hot spot. We may invert this expression to define a burn weighted average ion density of the hot spot.

$$n_{ion} = \sqrt{\frac{3Y_n}{4\pi \chi_D \chi_T \langle \sigma v(T) \rangle \tau R_{HS}^3}}$$

Once the average ion density is known, it straight forward to form expressions for each ignition parameter. The expression for ρRT^2 is:

$$\rho RT^2 = 1.3 \left(\frac{A n_{ion}}{N_0} \right) R_{HS} T^2 = 1.3 \frac{A}{N_0} \sqrt{\frac{3}{4\pi \chi_D \chi_T}} \sqrt{\frac{Y_n}{\tau R_{HS}}} \left(\frac{T^2}{\sqrt{\langle \sigma v(T) \rangle}} \right)$$

$$\rho RT^2 = 1.3 \times 2.741 \sqrt{\frac{Y_n(10^{15})}{\tau(ns) R_{HS}(\mu m)}} T^{-0.005}$$

The leading factor of 1.3 is a scale factor derived from ICF code simulations which forces the inferred values of ρRT^2 to agree with the code values. Next we need the mass of hot spot.

$$M_{HS} = \frac{4\pi}{3} R_{HS}^3 \rho_{HS} = \frac{4A}{N_0} \sqrt{\frac{\pi}{3}} \sqrt{\frac{Y_n R_{HS}^3}{\tau < \sigma v(T) >}}$$

$$M_{HS}(\mu g) = 1.7095 \times 10^{-11} \sqrt{\frac{Y_n(10^{15}) R_{HS}^3(\mu m)}{\tau(ns) < \sigma v(T) > (cm^3/sec)}}$$

Once the hot spot mass is known we can form the hot spot mass fraction.

$$M_f = \frac{M_{HS}}{M_{DT}}$$

M_{DT} is the total DT mass of the hot spot plus cold fuel and is known from the initial DT loading for a given shot. Once ρRT^2 and M_f are known the result of section 4 is used to form the ignition parameter β.

$$\beta = \frac{\rho R T^2}{14.2478 M_f^{0.2831}}$$

The pressure of the hot spot is also easy to find.

$$P_{HS} = 2K_B n_{ion} T = 2K_B \sqrt{\frac{3}{4\pi\chi_D\chi_T}} \sqrt{\frac{Y_n}{\tau R_{HS}^3}} \frac{T}{\sqrt{\langle\sigma v(T)\rangle}}$$

$$P_{HS}(GB) = 3.131 \times 10^{-6} \sqrt{\frac{Y_n(10^{15})}{\tau(ns) R_{HS}^3(\mu m)}} \frac{T}{\sqrt{\langle\sigma v(T)\rangle}}$$

Pτ is also easy to form. The hot spot pressure above is multiplied by the burn duration τ.

$$P\tau(GB \cdot ns) = 3.131 \times 10^{-6} \sqrt{\frac{Y_n(10^{15})\tau(ns)}{R_{HS}^3(\mu m)}} \frac{T}{\sqrt{\langle\sigma v(T)\rangle}}$$

It is also easy to find an expression for the χ ignition parameter defined in section 2.

$$\chi = \frac{P\tau}{(P\tau)_{ig}} = \frac{T_\alpha}{12} \sqrt{\frac{3}{\pi}} \sqrt{\frac{Y_n \tau}{R_{HS}^3}} \left(\frac{\sqrt{\sigma v(T)}}{T}\right) \left[\sqrt{4\chi_D\chi_T}\right]$$

$$\chi = 2.883 \times 10^{11} \sqrt{\frac{Y_n(10^{15})\tau(1ns)}{R_{HS}^3(\mu m)}} \left(\frac{\sqrt{\sigma v(T)}}{T}\right) \left[\sqrt{4\chi_D\chi_T}\right]$$

$$\chi \cong 42.92 \sqrt{\frac{Y_n(10^{15})\tau(1ns)}{R_{HS}^3(\mu m)}} T^{1.005} \left[\sqrt{4\chi_D\chi_T}\right]$$

The ignition parameter ITFX was designed specifically to measured directly from NIF data[4].

$$ITFX = \left(\frac{Y_n}{4.0 \times 10^{15}}\right) \left(\frac{DSR(\%)}{6.7\%}\right)^{2.1}$$

6. The Performance of Ignition Parameters in Simulations of NIF Capsules

In this section the performance of the three ignition parameters (χ, β and ITFX) are tested in numerical simulations of a relevant NIF design. The radiation drive of a simplified variant of the low-foot Revision-5 NIF design was randomly varied many times such that some of the calculations ignited and some of them didn't. Each random variation of the radiation drive was used to drive two separate calculations. In the first calculation the thermonuclear alpha particle deposited its energy normally into the hot spot and cold fuel. Such calculations will be known as the *alpha-on* simulations. In the second

calculation the alpha particle was not allowed to deposit any energy to the hot spot or cold fuel. This second class of calculations will be known as *alpha-off* simulations. The alpha-off simulations were then post-processed as synthetic data using the expressions listed in section 5 to produce inferred values for the three ignition parameters – χ, β and ITFX. This allows us to make scatter plots of the specific yield from the alpha-on simulations on the vertical axis and the inferred ignition parameter from the alpha-off simulations on the horizontal axis. Such plots will present clear evidence of the effectiveness of each ignition parameters.

Figure 6.1a shows the pie diagram of the capsule used in this study and figure 6.1b shows the nominal radiation temperature drive. This design is a simplification of the Revision-5 low-foot design tested many times on the NIF (also known as Rev-5). It is simpler than the Rev-5 design in that the ablator consists of a single layer of GDP CH with a constant concentration of silicon at 0.7% whereas in the Rev-5 design the ablator is divided into five separate layers with different silicon dopant concentrations.

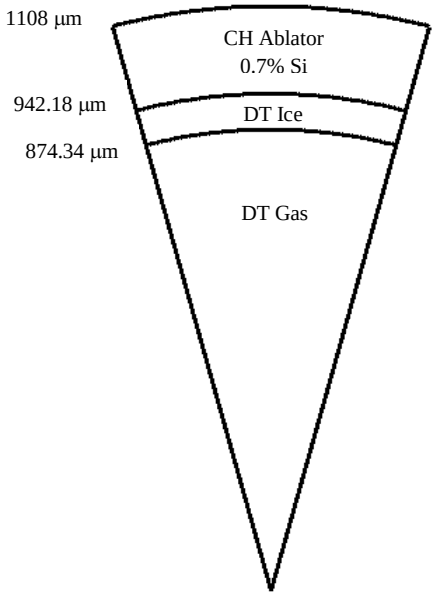

Figure 6.1a: Pie Diagram for Simplified NIF Capsule

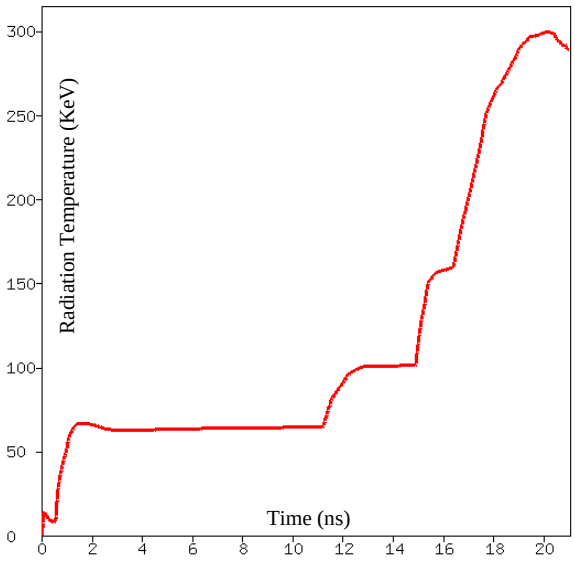

Figure 6.1b: Tr Drive for Simplified NIF Capsule

The radiation temperature shown in figure 6.1b is the Planck equivalent of a non-Planckian radiation source. It is a low-foot drive because the first temperature pulse is low and long. The temperature shown in figure 6.1b is the nominal drive intended to maximize the probability of ignition. This nominal drive was varied hundreds of times by raising or lowering the temperatures of the first, second, third or fourth pulses by random amounts. Most of the random drive variation decreased the probability of ignition.

The calculations were performed using CALEICF in one dimension. The computational features are listed here:

- Monotonic Sn Radiation Transport
- Lee-More Thermal Conductivity

- Opacities from LTE version of SHM (Screened Hydrogenic Model)
- EOS from LEOS tables (1018 DT, 5355 CH)
- Monte Carlo Charged Particle Transport
- KL 2006 Turbulence Mix[6] + ½ Bell-Plesset Terms
- Analytic M-Band spectral model for gold hohlraum
- 500 random variation in drive parameters
- Calculations post processed as synthetic experiments
- Both alpha-on and alpha-off calculations were made for each random drive variation

Before presenting the results for the three ignition parameters under study, figures 6.2 and 6.3 show examples of poor ignition parameters. Figure 6.2 shows the results for Pτ. Recall that the exact value of the ignition threshold for Pτ depends upon the temperature of the hot spot. This means that some capsules will ignite with Pτ values smaller than other capsules that fail to ignite. This behavior is displayed in figure 6.2. The ignition cliff for Pτ is smeared out. Renormalizing Pτ to form χ will fix this problem.

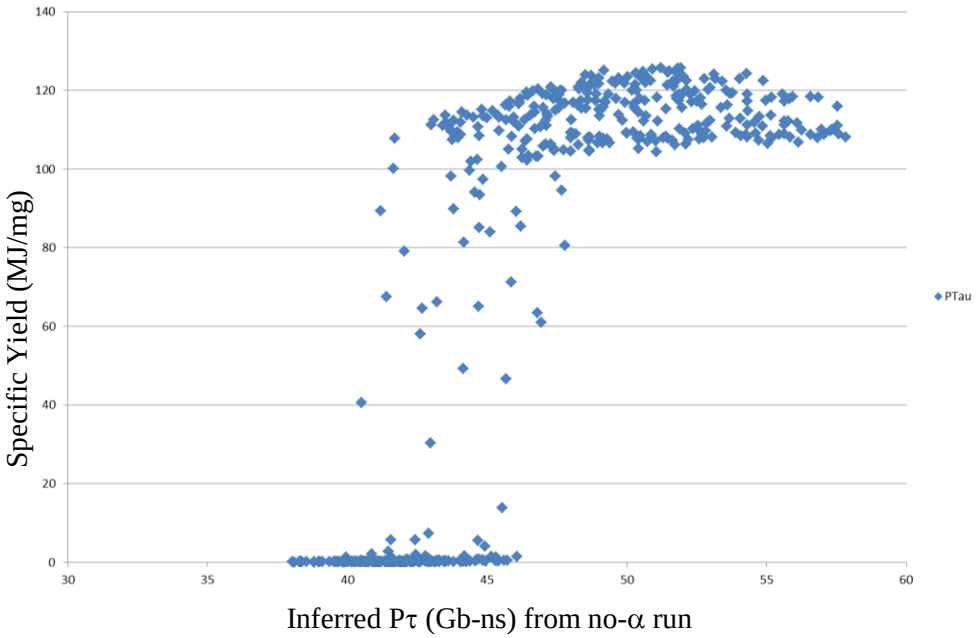

Figure 6.2: Specific Yield vs. Pτ.
Note the ignition cliff is smeared out.

Figure 6.3 show the specific yield versus the quantity ρRT. Three different series of calculations are plotted. The blue series represents the results using the KL mix model initiated with the expected surface roughness on the CH parts (~50nm). In the red series, the KL mix model was initiated with a CH surface roughness of 600nm. In the purple series, the KL mix model was initiated with a CH surface roughness of 1000nm. Increasing the initial surface roughness increases the mixing and degrades the performance of the capsule and hence it is no surprise that the ignition cliff drifts towards increasing ρRT with increasing mix. However if ρRT was a "good" ignition figure of merit, the ignition cliff should remain immobile as the mix is increased.

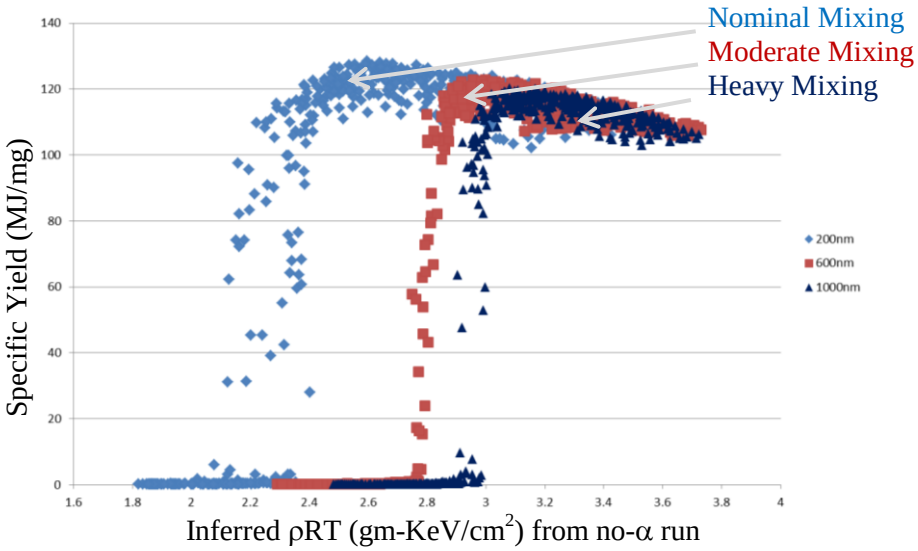

Figure 6.3: Specific Yield vs. ρRT.
The ignition cliff depends upon degree of mix.

Figures 6.4, 6.5 and 6.6 plot the specific yields as functions of the ignition parameters χ, β and ITFX. The specific yield is defined as the total thermonuclear yield divided by the initial mass DT in the capsule. It has units of MJ/mg. The specific yield is used rather than the total yield to facilitate the comparison of the ignition cliffs from small NIF capsules with that of larger reactor capsules.

All three of the ignition parameters perform well in the role of determining an ignition threshold – displaying sharp ignition cliffs with little or no change as the degree of mix is increased. However the ignition parameter β, shows a slight erosion of the ignition cliff with increased mix.

Two of the ignition parameters – β and ITFX – have already been normalized by simulations so it is no surprise that the ignition cliffs for these two parameters are close to unity. However there has been no explicit code normalization for χ. The Lawson Criterion is simply that $\chi > 1$. We see that the code simulations predict that the ignition threshold is closer to 1.2 rather than 1.0. This indicates rather close agreement between the code simulations and the original Lawson Criterion.

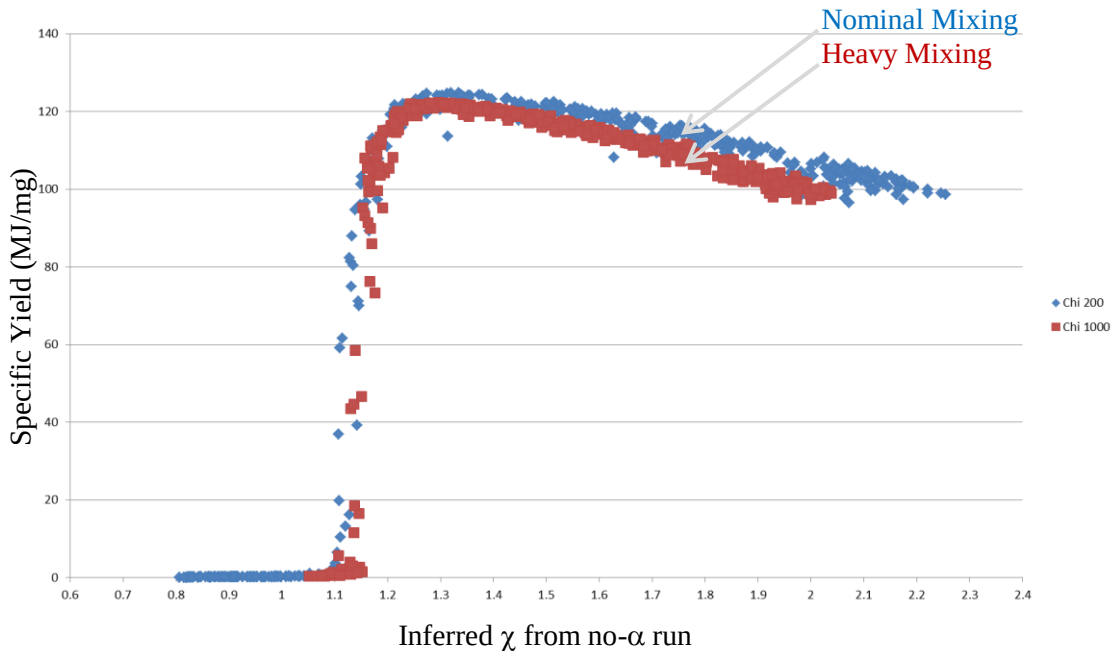

Figure 6.4: Specific Yield vs. χ.
The ignition cliff is sharp and does not depend upon degree of mix.

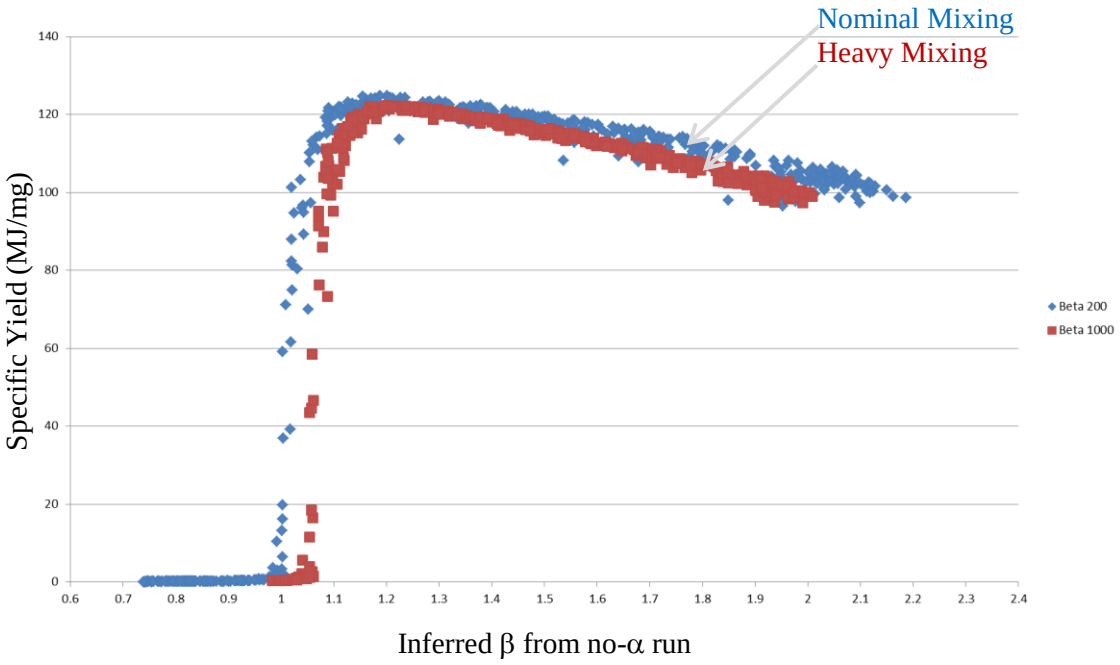

Figure 6.5: Specific Yield vs. β.
The ignition cliff is sharp and depends slightly upon degree of mix.

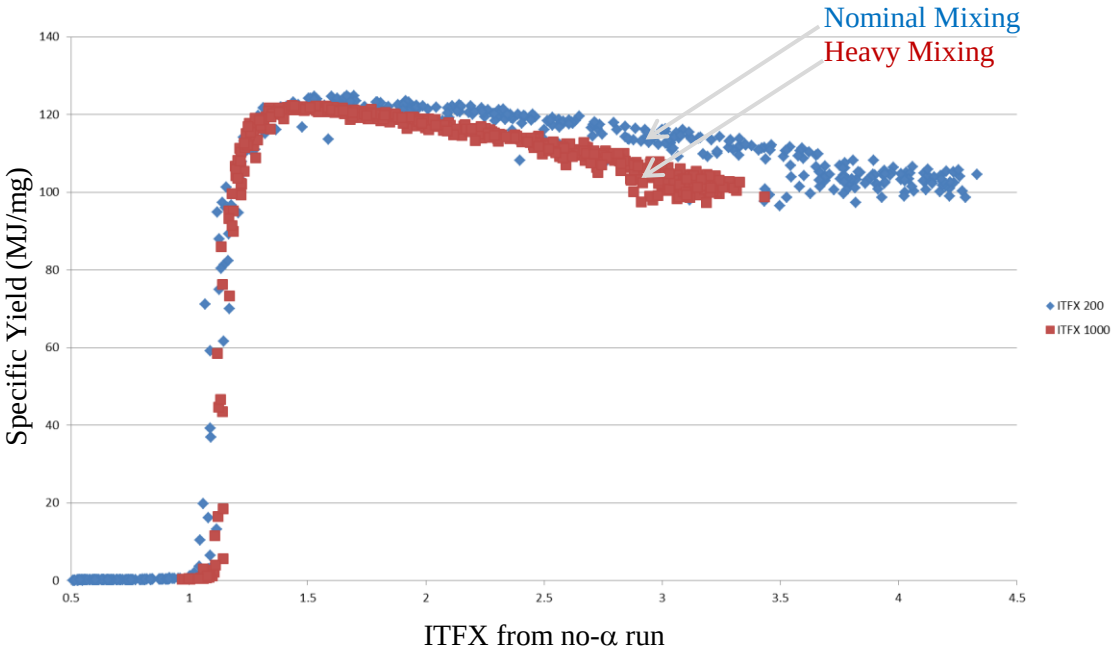

Figure 6.6: Specific Yield vs. ITFX.
The ignition cliff is sharp and does not depend upon degree of mix.

Figures 6.4 through 6.6 present the ignition cliffs as a function of alpha-off simulations. Unfortunately there is no way to turn off alpha deposition in the real world. But instead we can use the data base of simulations with random drive variations to establish the relationships between the ignition parameter with alpha-off and the ignition parameter with alpha-on.

Figure 6.7 presents the scatter plot of χ with alpha-on versus χ with alpha-off. Also plotted is the empirical fit.

$$\chi_{\alpha-Off} = 1.3\left(1 - exp(-0.77\chi_{\alpha-On})\right)$$

In much the same way figure 6.8 presents the scatter plot of β with alpha-on versus β with alpha-off. Also plotted is the empirical fit.

$$\beta_{\alpha-Off} = 1.11\left(1 - exp(-\beta_{\alpha-On})\right)$$

Finally figure 6.9 presents the scatter plot ITFX with alpha-on versus ITFX with alpha-off. Again there is also an empirical fit.

$$ITFX_{\alpha-Off} = \left[1.1\left(1 - exp\left(-0.90909(ITFX_{\alpha-On})^{1/1.94}\right)\right)\right]^{1.94}$$

Figures 6.7 through 6.9 show that the code simulations indicate a tight correlation between the ignition parameters with alpha depositions turned and turned off. The figures also show that the three empirical fits listed above, are reasonably accurate in capturing these three correlations. We will use these empirical fits in section 7 to transform inferred NIF ignition parameters with alpha depositions turned on into equivalent ignition parameters with alpha depositions turned off.

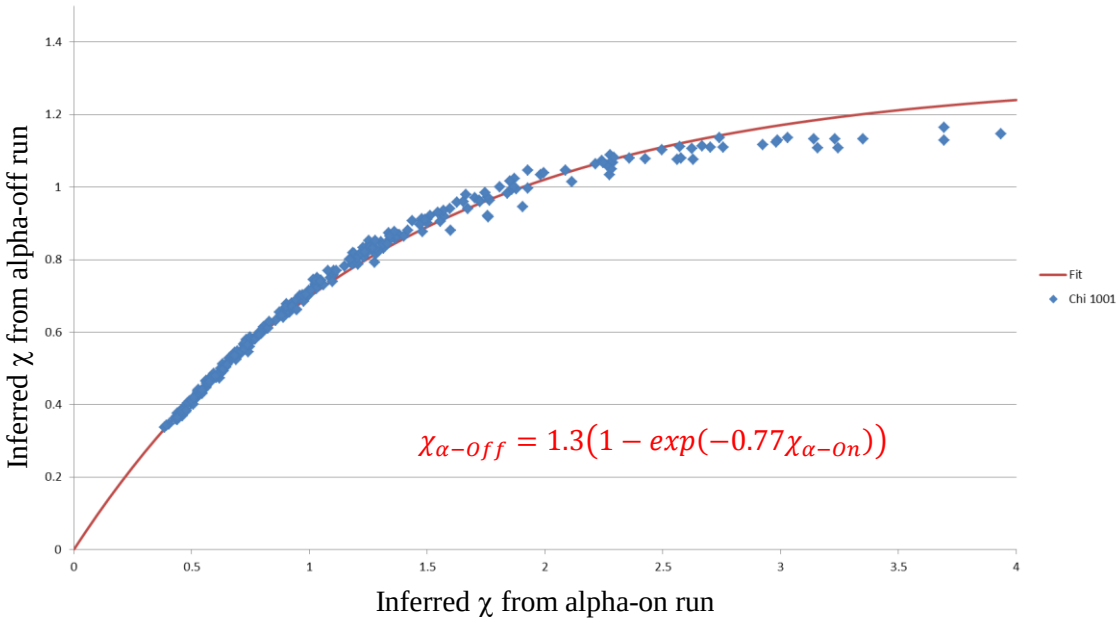

Figure 6.7: Scatter Plot χ(α-on) vs. χ(α-off) with Fit

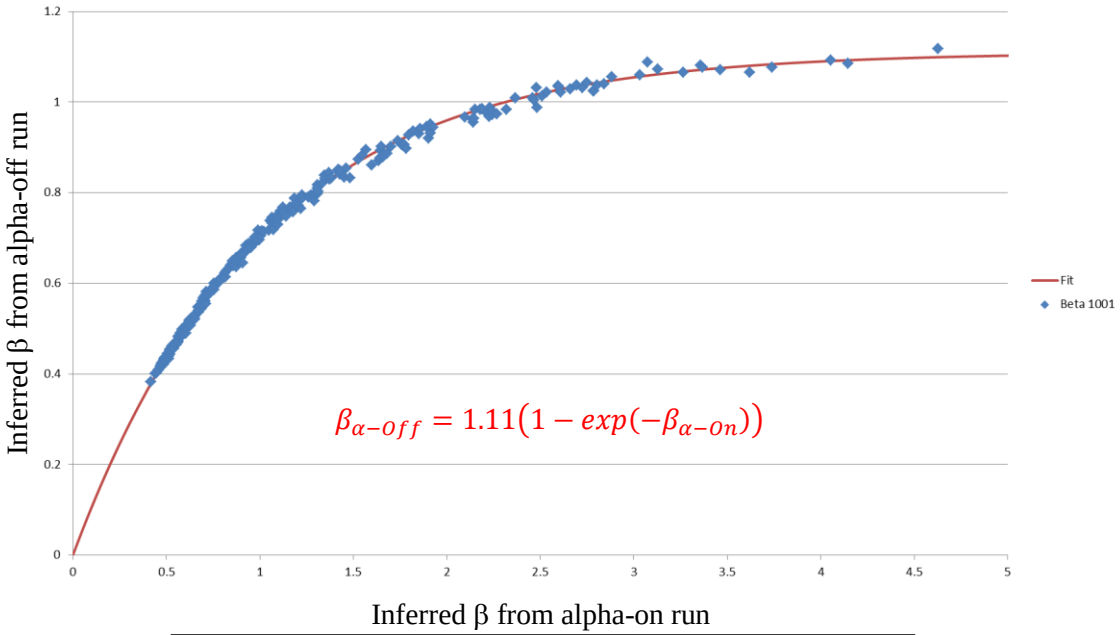

Figure 6.8: Scatter Plot β(α-on) vs. β(α-off) with Fit

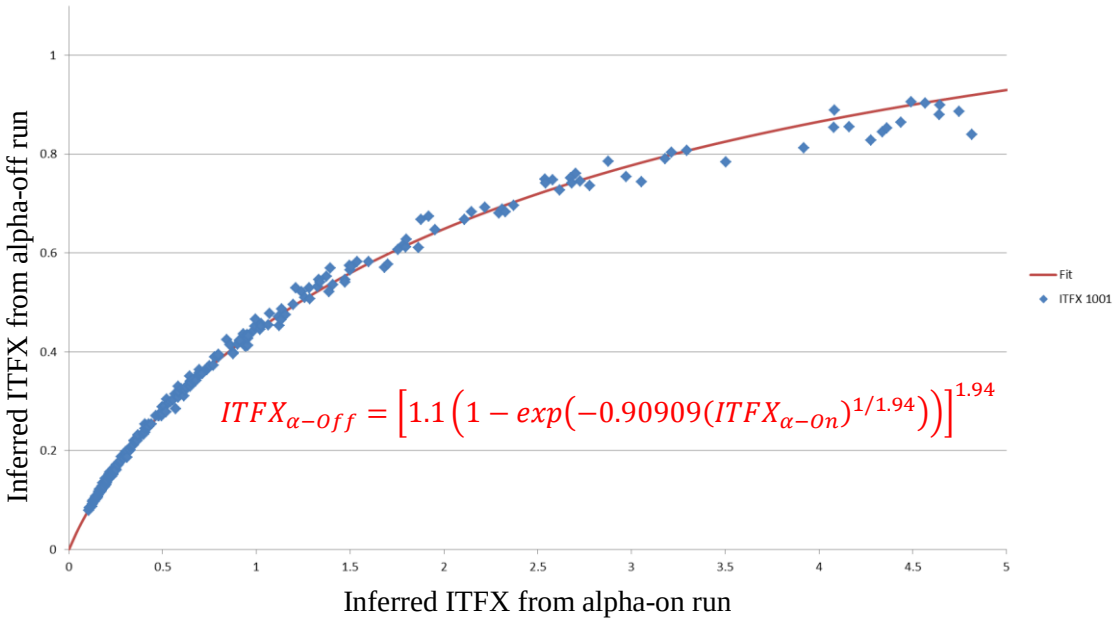

Figure 6.9: Scatter Plot ITFX(α-on) vs. ITFX(α-off) with Fit

7. Measured Ignition Parameters from NIF Shots

Now we can finally turn our attention to actual data taken from NIF shots. Table 7.1 lists the measured values for 25 DT layered shots fired on the NIF. Using the expressions developed in section 5 we can take these measured numbers and construct the values of the three ignition parameters which are listed in table 7.2.

Notice the two best performing shots in table 7.2 – highlighted in red – have χ values near 1.2 and yet they did not ignite. At first glance this appears to be in conflict with the simulation results of section 6 where we saw that ignition should occur for χ values above 1.2. However those simulation results were for χ values inferred from alpha-off runs. Recall that since there is no way to turn off alpha energy depositions in real data, the values listed in table 7.2 represent alpha-on numbers. We can use the empirical fits developed in section 6, to transform the ignition parameters with alpha-on into equivalent ignition parameters with alpha-off. The transformed alpha-off ignition parameters are listed in table 7.3. Notice that in terms of alpha-off, the χ values of the best performers are around 0.8 which we found in section 6 is close to, yet below the ignition threshold.

Figures 7.1 through 7.3 present the data in tables 7.2 and 7.3 in graphical form. In each of these figures squares represent code simulations discussed in section 6 and triangles represent the NIF data from tables 7.2 and 7.3. In all figures the vertical axis is the specific yield (MJ/mg). For the code simulations the specific yields are from the alpha-on calculations. In all figures the horizontal axis is one of the ignition parameters (χ, β or ITFX). Both alpha-on and alpha-off versions of the ignition parameters are plotted. The horizontal coordinates of the blue squares are the ignition parameters of calculations with alpha depositions turned on. The horizontal coordinates of the red squares are the ignition parameters of calculations with alpha depositions turned off. The horizontal coordinates of green triangles are the ignition parameters of the 25 NIF shots with alpha depositions turned on as listed in table 7.2. The horizontal coordinates of the purple triangles are the transformed ignition parameter of the 25 NIF shots with alpha depositions turned off as listed in table 7.3.

Table 7.1 Measured Data from 25 NIF Shots

Shot	Type	Yn	Tion	τ	R_{HS}	DSR
		10^{15}	KeV	ns	μm	%
110603	Low Foot	0.0642616	2.63884	0.220	25.3	4.326
110608	Low Foot	0.190962	3.10552	0.215	33.0	4.333
110615	Low Foot	0.43002	3.31903	0.215	38.4	3.537
110620	Low Foot	0.4113	4.3157	0.122	24.5	4.526
110826	Low Foot	0.17054	3.0617	0.180	25.0	3.880
110914	Low Foot	0.574	3.58679	0.171	28.3	4.880
111103	Low Foot	0.231342	3.2844	0.190	30.1	3.914
111112	Low Foot	0.602045	3.89828	0.154	30.9	4.211
111215	Low Foot	0.745	3.5325	0.180	28.0	4.307
120126	Low Foot	0.317184	2.87943	0.175	24.9	3.917
120131	Low Foot	0.620336	3.87902	0.199	32.7	3.698
120205	Low Foot	0.604543	3.43133	0.155	28.0	4.347
120321	Low Foot	0.415645	3.06822	0.158	26.0	6.258
130501	High Foot	0.767	3.02	0.172	37.9	2.960
130802	High Foot	0.48	2.85	0.216	38.9	2.840
130927	High Foot	4.42	4.43	0.188	35.4	3.660
131119	High Foot	5.237	4.77	0.156	37.2	3.800
140120	High Foot	8.002	5.58	0.170	35.2	3.900
140304	High Foot	8.125	5.83	0.168	33.9	3.820
140511	High Foot	6.1813	5.36	0.147	33.2	4.040
140520	High Foot	5.237	5.49	0.156	37.2	4.320
141123	Adia Shaped	1.1	3.40	0.108	25.7	5.450
131212	Diamond	1.83	3.55	0.161	33.0	2.300
140722	Diamond	0.371	3.38	0.198	38.9	2.080
140926	Diamond	2.80	3.84	0.154	36.6	2.200

Table 7.2: Inferred Ignition Parameters with Alpha-on

Shot	Type	Yn	Spec Y	β	χ	ITFX
		10^{15}	MJ/mg	---	---	---
110603	Low Foot	0.0642616	0.001034	0.1582	0.1025	0.0064
110608	Low Foot	0.190962	0.003011	0.1433	0.1413	0.0191
110615	Low Foot	0.43002	0.007253	0.1689	0.1815	0.0281
110620	Low Foot	0.4113	0.006819	0.3613	0.3386	0.0451
110826	Low Foot	0.17054	0.002804	0.1856	0.1826	0.0135
110914	Low Foot	0.574	0.009318	0.2842	0.3204	0.0738
111103	Low Foot	0.231342	0.003767	0.1776	0.1783	0.0187
111112	Low Foot	0.602045	0.009677	0.2917	0.2965	0.0568
111215	Low Foot	0.745	0.011971	0.3083	0.3745	0.0736
120126	Low Foot	0.317184	0.005258	0.2280	0.2304	0.0257
120131	Low Foot	0.620336	0.010266	0.2519	0.3119	0.0445
120205	Low Foot	0.604543	0.010070	0.2933	0.3042	0.0609
120321	Low Foot	0.415645	0.006581	0.2614	0.2523	0.0900
130501	High Foot	0.767	0.012599	0.2190	0.1997	0.0334
130802	High Foot	0.48	0.007867	0.1621	0.1592	0.0198
130927	High Foot	4.42	0.068884	0.5349	0.8118	0.3104
131119	High Foot	5.237	0.081617	0.6103	0.7946	0.3979
140120	High Foot	8.002	0.128041	0.8075	1.2603	0.6421
140304	High Foot	8.125	0.129543	0.8736	1.3759	0.6242
140511	High Foot	6.1813	0.098553	0.7933	1.0889	0.5342
140520	High Foot	5.237	0.083498	0.6707	0.8859	0.5209
141123	Adia Shaped	1.1	0.018234	0.3773	0.4845	0.1782
131212	Diamond	1.83	0.030521	0.3681	0.4494	0.0484
140722	Diamond	0.371	0.006079	0.1744	0.1504	0.0080
140926	Diamond	2.80	0.047319	0.4059	0.5145	0.0675

Table 7.3: Transformed Ignition Parameters with Alpha-Off

Shot	Type	β	χ	ITFX
		---	---	---
110603	Low Foot	0.1625	0.0987	0.0060
110608	Low Foot	0.1482	0.1340	0.0171
110615	Low Foot	0.1725	0.1696	0.0245
110620	Low Foot	0.3366	0.2984	0.0378
110826	Low Foot	0.1881	0.1705	0.0123
110914	Low Foot	0.2746	0.2842	0.0589
111103	Low Foot	0.1806	0.1668	0.0167
111112	Low Foot	0.2808	0.2654	0.0466
111215	Low Foot	0.2945	0.3257	0.0588
120126	Low Foot	0.2263	0.2113	0.0225
120131	Low Foot	0.2471	0.2776	0.0374
120205	Low Foot	0.2822	0.2715	0.0496
120321	Low Foot	0.2553	0.2295	0.0702
130501	High Foot	0.2183	0.1853	0.0296
130802	High Foot	0.1661	0.1500	0.0176
130927	High Foot	0.4598	0.6042	0.1955
131119	High Foot	0.5070	0.5949	0.2360
140120	High Foot	0.6150	0.8074	0.3320
140304	High Foot	0.6466	0.8494	0.3256
140511	High Foot	0.6079	0.7379	0.2922
140520	High Foot	0.5424	0.6428	0.2870
141123	Adia Shaped	0.3488	0.4048	0.1255
131212	Diamond	0.3418	0.3803	0.0404
140722	Diamond	0.1777	0.1422	0.0074
140926	Diamond	0.3704	0.4252	0.0544

Figure 7.1a plots the inferred NIF data and code results for the ignition parameter χ. If the code results were a good model of reality then we would expect to see the green triangles (alpha-on data) lay on top of the blue squares (alpha-on simulations) and we would also expect to see the purple triangles (alpha-off data) lay on top of the red squares (alpha-off simulations). There is some similarity between the simulations and the data but the proper symbols do not lay right on top of each other.

In figure 7.1b the same code results and data are plotted as in figure 7.1a only here we have assumed that the volume of the hot spot inferred from the P0 radius of the neutron pinhole image is too large and so we have reduced the hot spot volume in the formulae of section 5 by an arbitrary factor of ½. Notice that this improves the agreement between data and simulation.

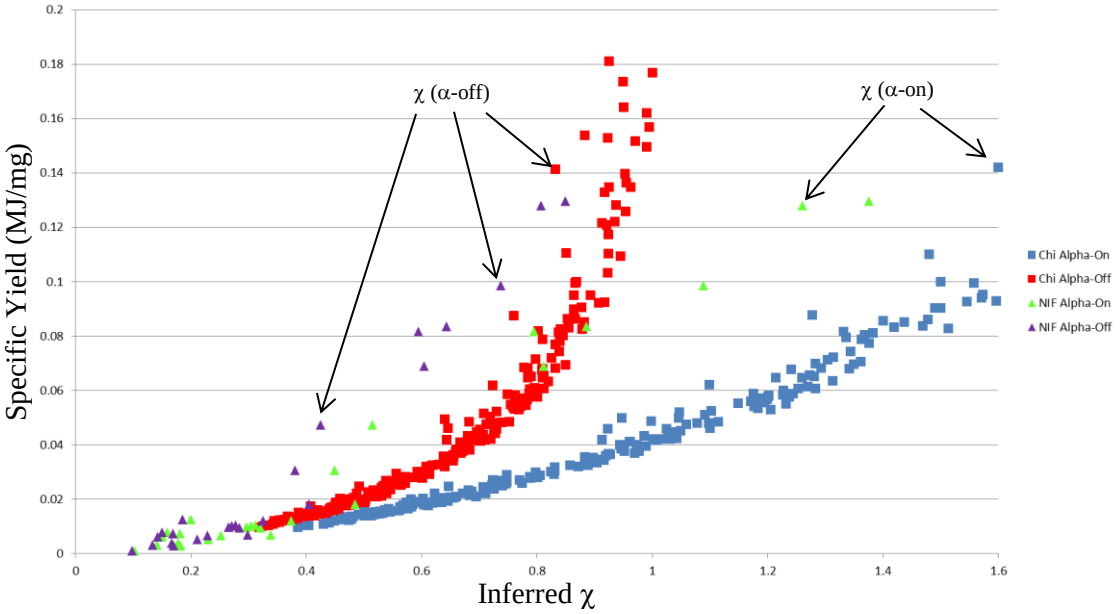

Figure 7.1a: Specific Yield vs. χ (α-on) & χ (α-off)

Triangles – NIF Data Squares – Code Simulations

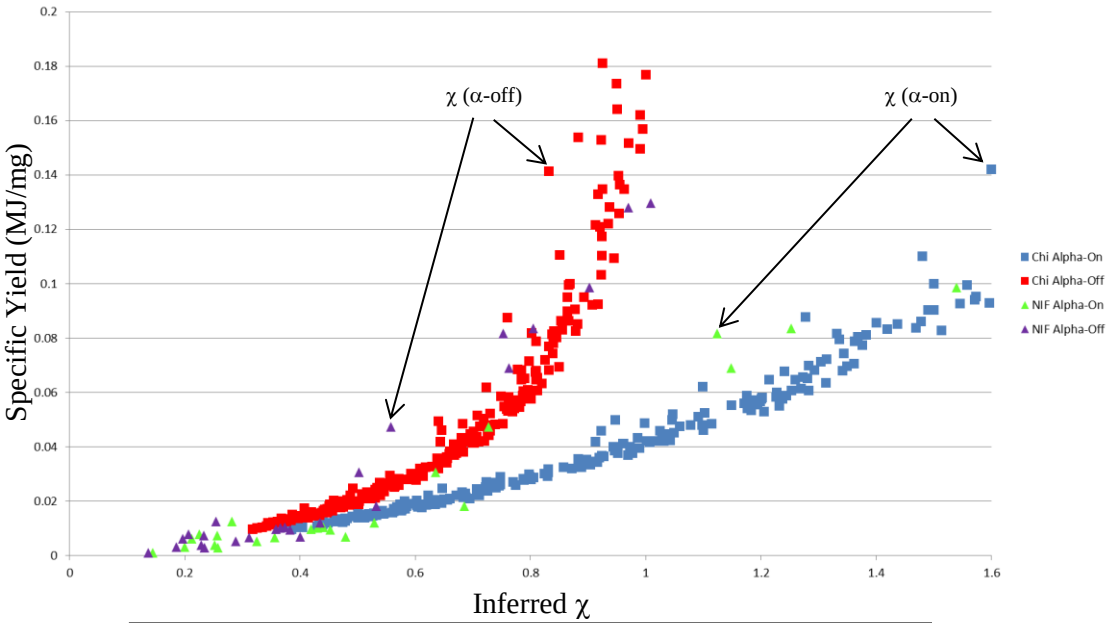

Figure 7.1b: Specific Yield vs. χ (α-on) & χ (α-off)

Triangles – NIF Data Squares – Code Simulations

The hot spot volume inferred from neutron pinhole image has been reduced by ½. This expands the value of χ by $\sqrt{2}$ and gives better agreement between simulations and data.

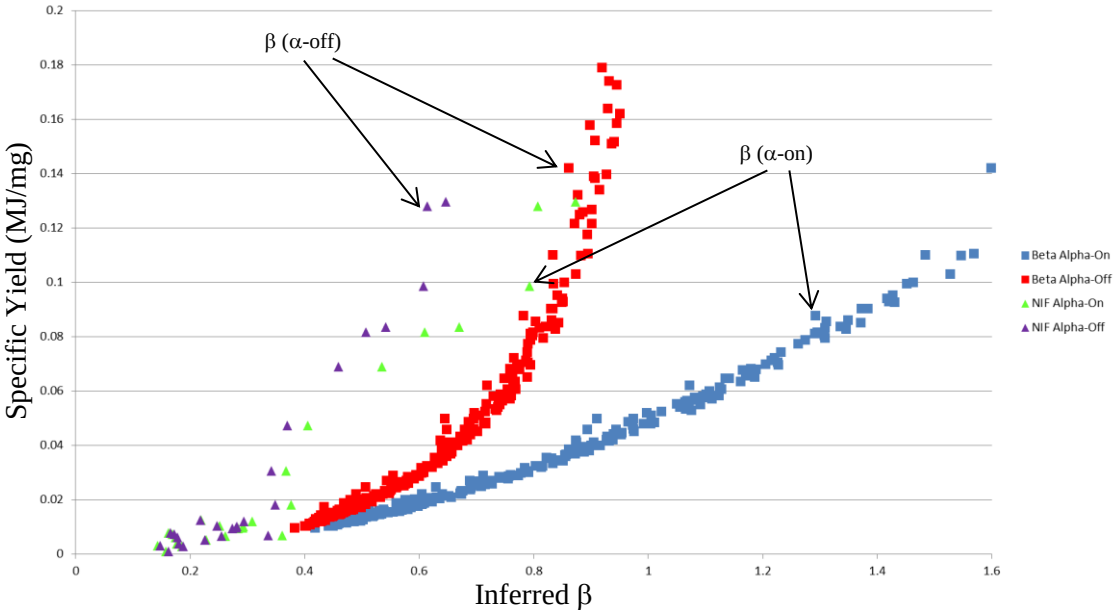

Figure 7.2: Specific Yield vs. β (α-on) & β (α-off)

Triangles – NIF Data Squares – Code Simulations

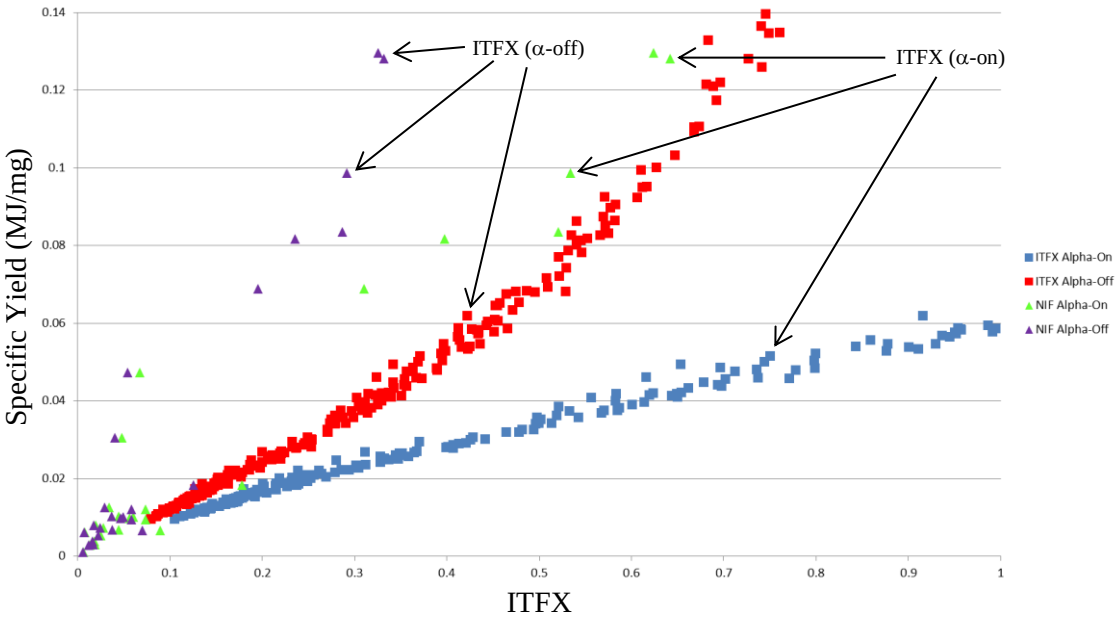

Figure 7.3: Specific Yield vs. ITFX (α-on) & ITFX (α-off)

Triangles – NIF Data Squares – Code Simulations

Figure 7.2 presents the results for data and simulations using β as the ignition parameter. Again we see data and simulation trending in similar ways, but the proper symbols do not lie on top of each other. The discrepancy between data and simulation for β in figure 7.2 is a little worse than it was for χ seen in figure 7.1a. Just as we saw in figure 7.1b, we could arbitrarily reduce the hot spot volume inferred from the NIF data and cause the data to stretch along the β axis, but in order to make the data fall on top of the simulations, the inferred hot spot volumes would have to be reduced by more than a factor of 2.

Figure 7.3 presents the results for data and simulations using ITFX as the ignition parameter. Once again the data and simulation trend in similar ways, but the discrepancy between data and simulation is even larger than we saw for either χ or β. I can't explain why the agreement between data and simulation for ITFX is not as good as it is for χ. Many ICF researchers at Livermore have compared data and calculations for ITFX over the last few years and find much better agreement. Perhaps I have made some mistake in the handling of ITFX.

8. Summary

In sections 2-4 and reference [4] we saw that all of the ignition parameters used in ICF research today can be derived from John Lawson's original ignition criteria proposed for magnetic fusion back in the 1950's. In section 6 we saw that in numerical simulations all of the ignition parameters perform well and perform about the same.

In section 5 we saw that all of the ignition parameters can be inferred more or less directly from data taken on NIF shots without the use of ICF code calculations. In section 7 the ignition parameters from 25 DT layered NIF shots were compared with the results from the code simulations of section 6. While all three ignition parameters displayed the same trends as the simulations, none of the ignition parameters produces an exact overlay between data and simulations. However, of the three ignition parameters, χ produced the best overall agreement between data and simulations.

Figure 8.1 is a slight variation of figure 7.1a. It shows the ignition cliff in terms of both χ with alphas on and with alphas off. Notice that the specific yields of the alpha-on and alpha-off simulations start to diverge near $\chi = 0.6$. This represents the onset of alpha heating. The code simulations in red squares predicts the steep part of the ignition cliff is between $\chi = 1.0$ and 1.2 with ignition beginning for $\chi > 1.2$. Figure 8.1 allows us to naturally divide the ignition space into three slightly arbitrary regions.

1) The No Alpha Heating Region for $\chi < 0.6$
2) The Alpha Heating Region for $0.6 < \chi < 1.2$
3) The Ignition Region for $1.2 < \chi$

Figure 8.1 indicates that many of the early NIF shots fell into the no alpha heating region with $\chi < 0.6$. The figure also indicates that several of the later NIF shots fell well into the alpha heating region with χ values near 0.85. Figure 8.1 also indicates that the best performers are near the foot of the steep part of the ignition cliff. Lastly figure 8.1 suggests that if we could double the alpha-off value of χ we would be very likely to cross the ignition threshold. There are several ways to double the value of χ, but the most obvious way would be to increase the hot spot pressure by increasing the spherical symmetry of the hot spot.

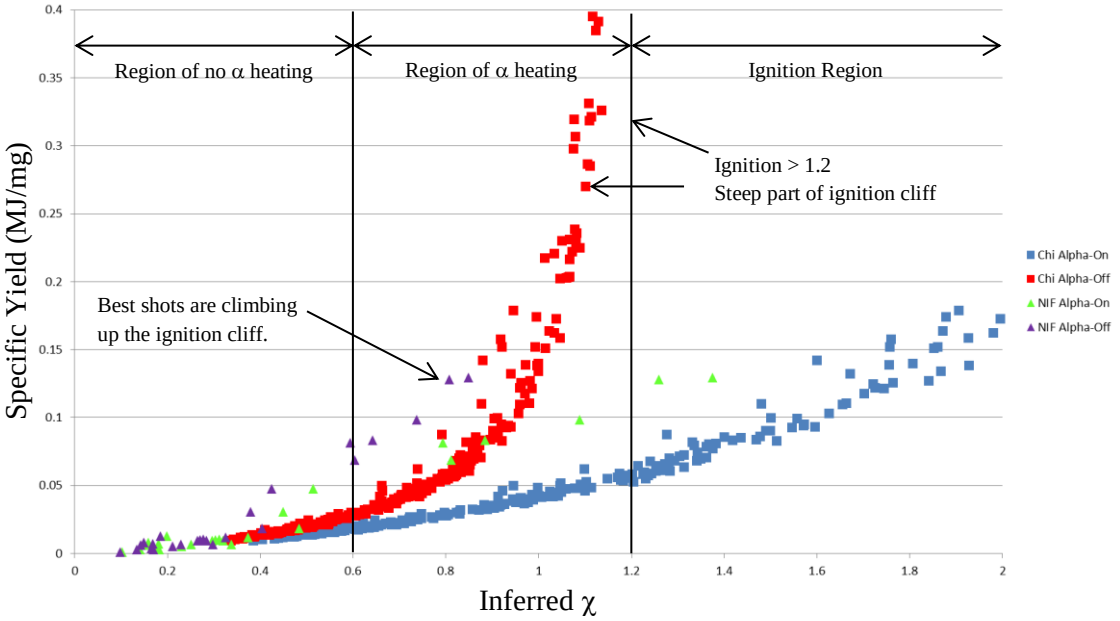

Figure 7.4: Specific Yield vs. χ (α-on) & χ (α-off)
Triangles – NIF Data Squares – Code Simulations

The α-on and α-off simulations diverge around χ = 0.6 indicating the onset of α heating. The steep part of the ignition cliff is between χ = 1 and χ = 1.2. Best NIF shots are into the α-heating region and near the bottom of the steep rise in the ignition cliff.

Acknowledgement: I would like to thank Oleg Schilling for suggesting I take on this subject. This work was performed under the auspices of the U.S. Department of Energy by Lawrence Livermore National Laboratory under Contract DE-AC52-07NA27344.

References

[1] J. D. Lawson, "Some Criteria for a Power producing thermonuclear reactor", (Technical Report). Atomic Energy Research Establishment, Harwell Bershire, U.K.A.E.R.E. GP/R 1807 (December 1955).

[2] Ricardo Betti, et al, "Thermonuclear ignition in inertial confinement fusion and comparison with magnetic fusion", *Plasma of Physics* **17**, 058102 (2010).

[3] Baolian Cheng, Thomas J. T. Kwan, Yi-Ming Wang & Steven Batha, "On the thermonuclear ignition criterion at the National Ignition Facility", LA-UR-14-24110, August 5, 2014.

[4] John Lindl, Otto Landen, John Edwards, Ed Moses, "Review of the National Ignition Campaign 2009-2012", *Physics of Plasmas* **21**, 020501 (2014).

[5] Paul Springer & Charles Cerjan, "Evaluation of Symcap and THD Performance", LLNL-AR-466575, January 20, 2011.

[6] Dimonte & Tipton, "K-L turbulence model for Rayleigh-Taylor and Richtmyer-Meshkov instabilities" *Journal of Fluids*, **18**, 085101 (2006)